Developments in the Built Environment 18 (2024) 100446

Contents lists available at ScienceDirect

Developments in the Built Environment

journal homepage: www.sciencedirect.com/journal/developments-in-the-built-environment

Design of an electric activation system for the smart hybrid tendons crack-closure system in concrete beams.

Brunella Balzano [a,*], Shahram Sharifi [b], John Sweeney [c], Glen Thompson [c], Cristina de Nardi [b], Tony Jefferson [b]

[a] Cardiff University, Welsh School of Architecture, Bute Building, King Edward VII Ave, Cardiff, CF10 3NB, UK
[b] Cardiff University, School of Engineering, Queen's Buildings, 14-17 The Parade, Cardiff, CF24 3AA, UK
[c] University of Bradford, Bradford, BD7 1DP, UK

ARTICLE INFO

Keywords:
Self-repairing
Concrete
Service life
Durability

ABSTRACT

This work presents the design of a smart activation system for the crack-closure technology of the Hybrid Tendons. Previous research has demonstrated the effectiveness of this technology in providing a self-repairing mechanism for concrete elements. The Hybrid Tendons are made combining a pre-stressed Kevlar inner core restrained by a Shape Memory Polymer sleeve. To trigger the crack-closing action, the Shape memory potential of the outer sleeve needs to be activated via heating. The work focuses on the design and testing of an electric activation system for the Hybrid Tendons using a system of heating wires. Kanthal wires are chosen for this application and integrated in the manufacturing process of the Hybrid Tendons: the wires are wrapped around each tendon and connected to a power supply. An experimental campaign is conducted to assess the system's capability to activate the Hybrid Tendons and deliver the crack-closing action in concrete beams under constant load. Additionally a numerical model is also developed to offer a sound interpretation of the experimental results. The system is ultimately proven successful in activating the Hybrid Tendons embedded in the concrete, effectively delivering the crack-closing action and boosting the flexural response of the structural element.

1. Introduction

It is a matter of major concern that many existing concrete structures worldwide are in a state of premature deterioration and distress, giving rise to poor durability performance (Vaysburd et al., 2004), (Dawood et al., 2020), (Alexander and Beushausen, 2019). Expectations of extended service life are now increasing, and they are reflected in the modern design codes currently aiming for service lives of more than 50 years for concrete structures in large public works (Alexander, 2018). However, it was shown that even much modern structures, exposed to the combined effects of mechanical loads and severe service conditions (i.e. temperature fluctuations, severe weather and pollution), begin to deteriorate after only 20 or 30 years (Beushausen et al., 2019).

Infrastructures built with ordinary Portland cement concrete are known to have a short service life and poor durability, both closely related to concrete cracking (Mindess et al., 2003), (Angst, 2019), (Althoey et al., 2022). Cracking can present at different stages of a structure's lifetime and is usually caused by physical, chemical, and mechanical interactions between concrete and its service environment, (Dai et al., 2020), (Shen et al., 2020). The short service life of concrete may lead to a series of negative effects: deteriorated infrastructures need new materials for repair and maintenance which place enormous strain on construction budget, along with the associated carbon emissions from construction-related traffic (Yildirim et al., 2018).

As a solution to the challenge of cracking in concrete, self-healing technologies offer an innovative and promising solution with the potential to increase the durability and service life of the built environment thereby reducing the need for maintenance and decreasing the environmental impact (Cappellesso et al., 2023). Research on self-healing concrete has been widely explored by many researchers (Bekas et al., 2016), (Danish et al., 2020), (Gupta et al., 2018), (Kumar Jogi and Vara Lakshmi, 2021), (Hossain et al., 2022), (De Nardi et al., 2023), (Shields et al., 2024): various self-healing technologies have been applied to a wide range of cementitious materials and shown many progresses in dealing with a diverse range of crack widths.

Concrete has a natural crack-healing capability and this is known as

* Corresponding author.
E-mail address: balzanob@cardiff.ac.uk (B. Balzano).

https://doi.org/10.1016/j.dibe.2024.100446
Received 25 September 2023; Received in revised form 2 April 2024; Accepted 23 April 2024
Available online 7 May 2024

"autogenous" healing. Substantial research has been undertaken to enhance this phenomenon and boost concrete durability (De Belie et al., 2018), (Neville, 2002), (Edvardsen et al., 2015). However, "autogenous" healing can only take place if certain conditions are satisfied: in particular, the width of the crack is a determining factor which greatly affects this process (De Belie et al., 2018), (de Rooji et al., 2013).

When the crack width becomes too large for the autogenous healing to take place (i.e. >0.1 mm) then mechanisms of "autonomous or autonomic" healing (Minnebo et al., 2017), (Wu et al., 2012) which use engineered mechanisms added to the structural element to provide the crack-closing action (Han et al., 2015), offer an effective remedy to combat cracking.

Balzano et al., 2021 (Balzano et al., 2021) presented a novel crack-closure system for cementitious structural elements consisting of pre-tensioned hybrid tendons. The tendons are made combining a pre-stressed inner core of aramid fibre ropes, and a shape memory PET outer sleeve, able to shrink upon activation via heating. During manufacturing, the tendon's inner core is put into tension and the outer sleeve into compression, such that the tendon is in equilibrium. When cast in a cementitious structural element and heat activated, the shrinkage potential of the PET sleeve is triggered, in turn releasing the stored inner core strain energy. The released tension applies a compressive force to the cementitious element, in which the tendons are embedded, closing any cracks that have formed perpendicular to the axis of the tendons.

The Hybrid Tendons were proven successful in closing structural cracks up to 0.3 mm which is the UK standard value for a serviceability crack width (Wiktor and Jonkers, 2011), (Medeiros-Junior, 2018). Moreover, hybrid tendons have the added value of acting as effective reinforcement both before and after the release of the crack-closing action.

While proven effective, the Hybrid tendons are not ready yet to be used in a working structure. Previous studies successfully demonstrated the concept of hybrid tendons, laying the foundation for improvements in various aspects. For instance, using an oven to activate the system presented a drawback as the structural element was not under load during the process. Additionally, a non-local control of the heating subjected the entire element to unnecessary and potentially hazardous temperature increases, resulting in energy inefficiency as well. One missing element in this system is a dedicated remote activation system capable of triggering the shrinkage of the PET sleeve, subsequently releasing the stored stress.

This work focuses on technological improvements to facilitate upscaling and readiness for real-world applications. A purpose-designed electric heating system has been developed and strategically integrated into the concrete elements, with no significant geometry variations. The system triggers the tendons within the concrete to autonomously close cracks while selectively heating only the tendons and the adjacent part of the element in contact with them. This is accomplished through an electrical system meticulously crafted using Kanthal, precisely activating the tendons when the concrete elements, integral to the structure, are under load.

A similar system was already developed by Teall et al., (2018) (Teall et al., 2018a) for a different type of PET tendon with PET in the form of fibres. In this previous attempt, Nichrome wires were used to generate the activation temperature to trigger the PET shrinkage which in turn would generate the compressive action necessary to close the concrete cracks. However, challenges were encountered in achieving the activation temperature across all of the PET filaments. Moreover, the electric wires seemed to produce an interference with the steel reinforcement also needed in the concrete beam. In addition, these PET tendons did not provide significant flexural reinforcement.

This paper describes the experimental work carried out to prove the efficacy of Kanthal heating wires as activation system for the Hybrid Tendons in structural concrete beams. This work also presents a numerical model based on the concept of non-linear beam-hinge used to interpret the experimental results. The paper layout begins with a general introduction to the concept adopted for the activation system and the design of the experimental campaign. Following a description of the materials used in the laboratory experiments (Section 2-3), the set up of the experiments and the stages of the testing are then reported in Section 4. The numerical model is described in Section 5 and the experimental and numerical results are then discussed in Section 6. The paper concludes with a final conclusive section reporting the main achievements of this research.

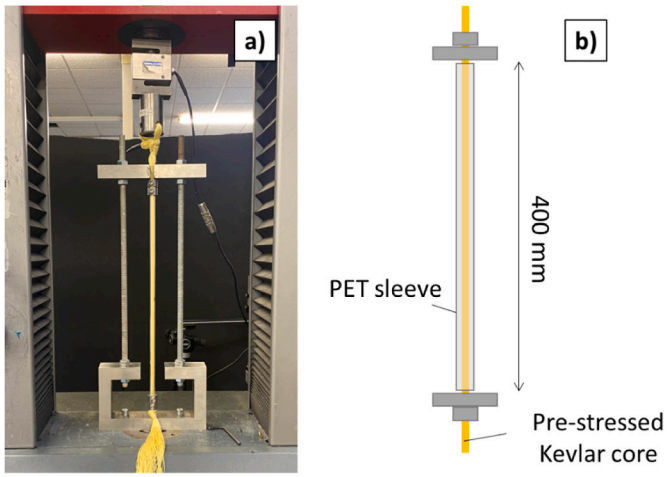

Fig. 1. a) Apparatus designed to pre-stress the Hybrid Tendons inner core. The system was mounted on a Zwick Z050 with a 100 kN Loading cell. b) Sketch of the constitutive elements of the Hybrid Tendons.

2. General concept

The present work follows up on the progress of the previous research on Hybrid Tendons (Balzano et al., 2021) by applying them in concrete beams of an upscaled size compared to our previous work (100x100x500mm) and investigating the viability of activating via a heating system embedded in the beam together with the tendons.

2.1. The hybrid tendons

The Hybrid Tendons were manufactured according to a procedure similar to the one reported in Balzano et al., 2021. The Kevlar inner core was pre-stressed using the apparatus reported in Fig. 1a. The tendon inner core was connected to a Loading cell, restrained at the top by means of a steel framing system and with the lower anchorage clamped in place. The inner core was then pre-stressed up to a designed value and then restrained within the PET shape memory tube, storing the necessary force that would be released at activation and promote a post-compression in the structural element (Fig. 1b). Each tendon is 400 mm long and is made of a PET outer sleeve and an inner core of 6.3 mm diameter Kevlar Ropes, with an average pre-stress per tendon of 1500 N.

The choice of Kevlar ropes for the Tendons' inner core lies on the finding of previous studies showing the potential of this material to act as effective reinforcement for concrete elements (Dolan, 1991).

It is worth mentioning that during the pre-stressing procedure, the PET tube would experience some bending under the compressive action of the inner core. The deformation is however self-restrained by the inner core itself, having the latter to retain its state of pure tension.

The PET is a shape memory polymer manufactured using a die-drawing process (Balzano et al., 2021). The shrinkage potential of the PET sleeves is activated when they are exposed to a temperature of approximately 100° C, and reaches a maximum at a temperature of between 120 and 130° C.

The geometrical and mechanical properties of the different

Table 1
Material Properties of the constitutive elements of the Hybrid Tendons.

Kevlar Core		
Core Nominal Diameter	*mm*	6.3
Tensile Strength	*MPa*	600.0
PET Outer Sleeve		
Outer Diameter	*mm*	11
Thickness	*mm*	2.4
Tensile Strength	*MPa*	90.0

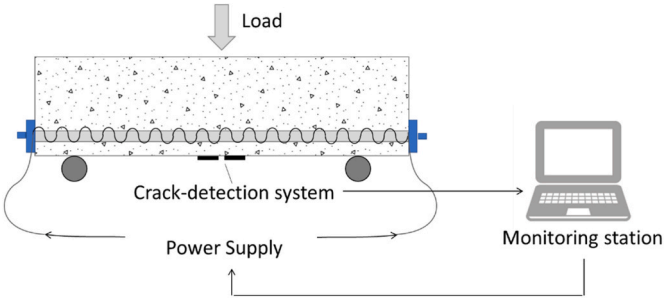

Fig. 2. Scheme of the activation system adopted for the Hybrid Tendons system.

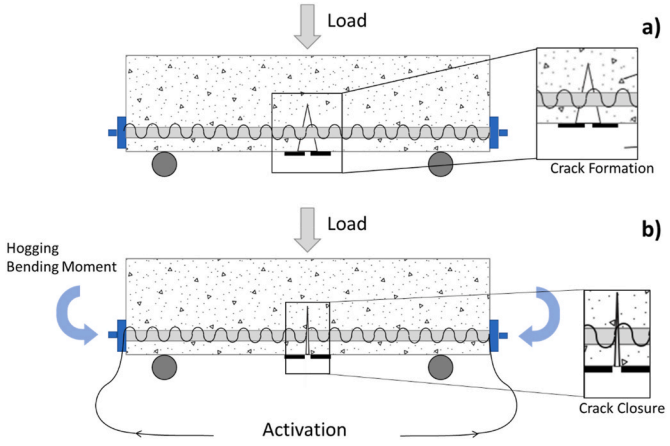

Fig. 3. Working Phases of the embedded hybrid tendons and related activation system.

components of the Hybrid Tendons are reported in Table 1.

2.2. Activation system

The heating system presented in this work consisted of Kanthal heating wires wrapped around each tendon and externally connected to a power supply. The whole system was then connected to a computer for data collection and to control the activation. The general scheme of the experiment setting is represented in Fig. 2.

One of the main challenges explored in the framework of this work was to assure the delivery of the crack-closing action while the Load was still active on the structural element, hence reproducing what would actually happen in a real-world application. In the previous experimental campaign, Balzano et al. (2021) neglected this aspect, only focusing on demonstrating the potential of the hybrid tendons as a crack-closure technology. The activation was indeed sought through oven heating, once the samples were removed from the loading frame.

For this work the samples were first loaded in three-point bending in displacement control, to induce a crack (Fig. 3a). Once the crack width

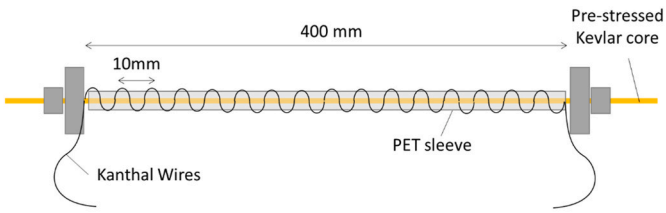

Fig. 4. Hybrid Tendons with Kanthal wires prepared to be casted within the concrete specimens.

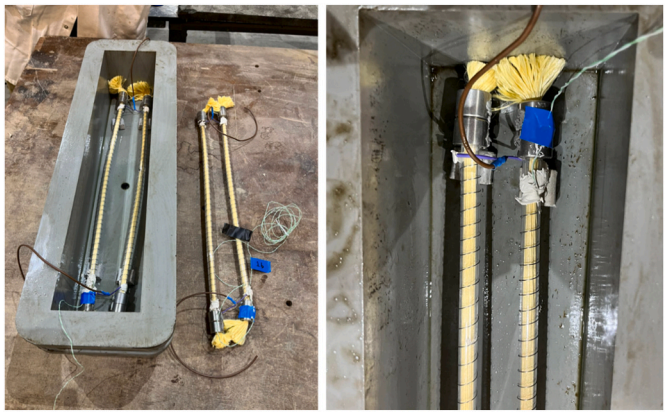

Fig. 5. Positioning of Hybrid Tendons before casting and close-up on the use of glue to keep the Kanthal wires in place.

reached a desired value, the test was switched to load control, keeping the load constant on the beam, while the activation process took place. In activating the tendons, the stored pre-stress was released, generating a hogging bending moment which counteracted the effect of the mid-span loading, allowing the reduction of the crack-width (Fig. 3b).

The electrical activation system was designed using high resistivity Kanthal wires. Kanthal is a iron-chromium-aluminium (FeCrAl) alloys used in a wide range of resistance and high-temperature applications. It is well known for its flexibility, tensile strength and oxidation resistance and already used in concrete to perform diverse thermal studies (Sales et al., 2010), (Kanthal, 2003). In this system, Kanthal wires 24 AWG (Average Wire Gauge) were used with a nominal diameter of 0.5 mm and resistance of 7.23 Ohm/m.

The Kanthal wire was wrapped around each tendon to form a coil resistance, generating the heat necessary for the activation, as depicted in Fig. 4. Notably, a pitch of 10 mm was chosen for this purpose, determined through experiments conducted by the authors. It was found that the optimal pitch for a set of four tendons, operating at a maximum voltage of 20 V, was 10 mm. Pitch sizes below 10 mm led to tendon melting, whereas sizes exceeding 10 mm proved ineffective in producing the required heat for PET shrinking.

To ensure the preservation of the coil's original shape and maintain the desired spacing between wire turns (coil spaces), the coil was glued to both ends of the tendon securely (Fig. 5). For this purpose, an

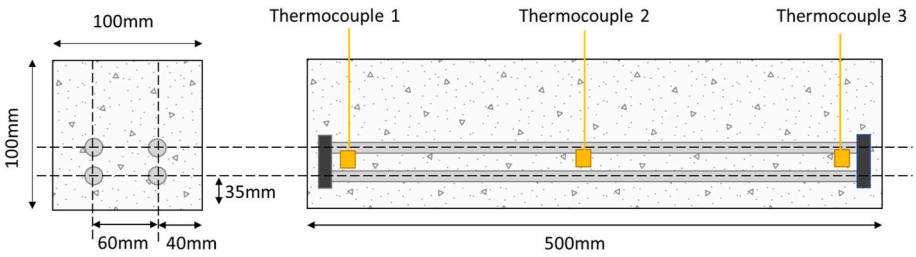

Fig. 6. Geometry of the concrete specimes and positions of the thermocouples.

appropriate adhesive with thermally conductive, good dielectric properties, and high-volume resistivity (AS1803 SILCOTHERM) was used. This specific adhesive offers efficient heat transfer from the coil to the tendon while possessing non-corrosive properties. These desirable qualities make it an excellent choice for integration into an electrical activation system, ensuring optimal performance and functionality (CHT UK Bridgwater LTD). The Kanthal wires were externally connected to a DC Supply (Aim-TTi CPX400DP Bench Power Supply) remotely controlled via a computer system connected to a data logger, recording the resistance, temperature and load.

3. Concrete mix

The concrete mix design for the beam specimens was prepared using Portland cement CEM II A/L 32.5 R (CAS number 65997–15-1), standard quartz sand (CAS number 14808–100 60–7) as fine aggregate, 10 mm aggregates and tap water. Cement (c), sand (s) and aggregates were mixed in a ratio of 1:1.55:2.1 by mass, and water (w) was added at a w/c ratio of 0.55 by mass. The mix proportion of cement, sand, aggregates and water were 329.4 kg/m^3, 510.6 kg/m^3, 691.7 kg/m^3, 181.2 kg/m^3 respectively. The selected mix design is consistent with previous research on the tendons, maintaining uniformity across the study. The primary goal was to create a concrete mix with decreased strength deliberately. This common approach in the field of self-healing concrete (Teall et al., 2018b) was employed to intentionally make the beam susceptible to damage. Following the procedure by BS EN 12350–1:2000 and BS EN 12390–6:2009, the compressive strength (f_{cu}) and tensile splitting strength (f_{cyl}) of the concrete mix were determined by casting and testing three 100x100 × 100mm cubes and three Ø100 × 200mm cylinders. The specimens were promptly covered with damp hessian for 7 days. The decision to opt for wet hessian over a water tank was driven by safety considerations due to the electrical aspect of the experiment. The specimens were removed 2 h prior to the test to allow them to reach room temperature. It was found that the compressive strength had a mean value of 29.2 MPa with a coefficient of Variation of 0.02, while the tensile splitting strength had a mean value of 3.48 MPa with a coefficient of variation of 0.08.

The testing age at 7 days was consistently maintained throughout the study, i.e. tensile, compression, and flexural tests. This approach ensured uniform testing conditions, contributing to the reliability of the experimental results. The goal of this investigation was to evaluate the system's ability to activate the crack closure of concrete samples under loads. The assessment of the concrete matrix at the 7-day mark demonstrated sufficient strength to illustrate the system's behaviour. It is noteworthy that prior tests with a comparable mix design indicated that by the 7th day, the concrete had already achieved the most of its strength (Edvardsen, 1999), (Jefferson et al., 2010).

4. Experimental campaign

4.1. Beam specimens

Four 100x100x500mm beams were prepared with four tendons embedded in each sample. Each tendon was manufactured with an initial pre-stressing force of 1.5 kN (±200 N) which gave a total average initial pre-stress ($P_{r,0}$) of 6 kN. Three Type-K thermocouples were also embedded in each beam and positioned along the tendons to monitor the temperature change once the activation process started. Type- K Thermocouples have been widely used in the years for concrete temperature monitoring on structures at different scales (Kwan et al., 2013), (Chang et al., 2009); indeed, they give a good approximation of the gradient change within the concrete which would be sufficient for the aim of this application.

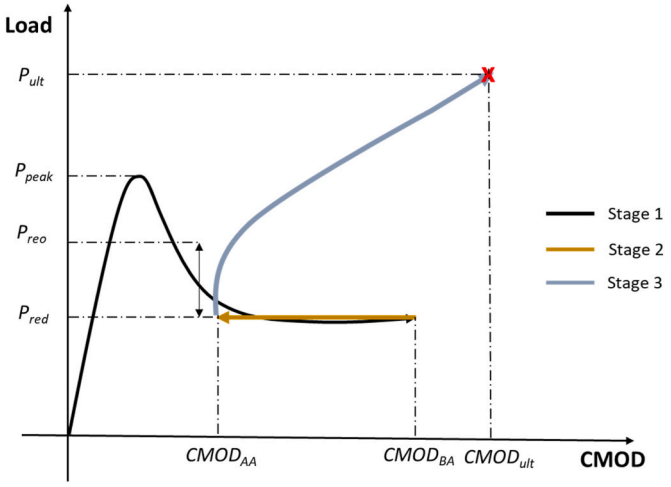

Fig. 7. General Loading scheme of the 3-point bending test and stages of the test.

Fig. 6 shows a general scheme of the beam specimen with embedded tendons and the position of the thermocouples. In order to meet the minimum concrete cover specified by BS 8500 for non-severe environments, a spacer with a height of 25 mm was employed. Taking into account the 10 mm radius of the clamps at the tendon's ends, the ultimate distance from the tendon's centre to the bottom of the beam is 35 mm.

4.2. Testing stages

The testing procedure comprises three stages, which are described below and illustrated schematically in Fig. 7.

Stage 1: The specimen was loaded in 3-point bending test to induce a crack with the selected crack mouth opening displacement (CMOD). The CMOD was measured via a clip gauge transducer which was mounted on the underside of each beam specimen and provided feedback to the load actuator. This stage is characterized by an initial linear behaviour of the beam, prior the formation of the crack. In the Load/CMOD graph the load would show an initial peak (P_{peak} in Fig. 7) which highlighted the end of the elastic behavior of the concrete and the initiation of the crack. After the first crack opening then the specimen experienced a softening phenomenon which in

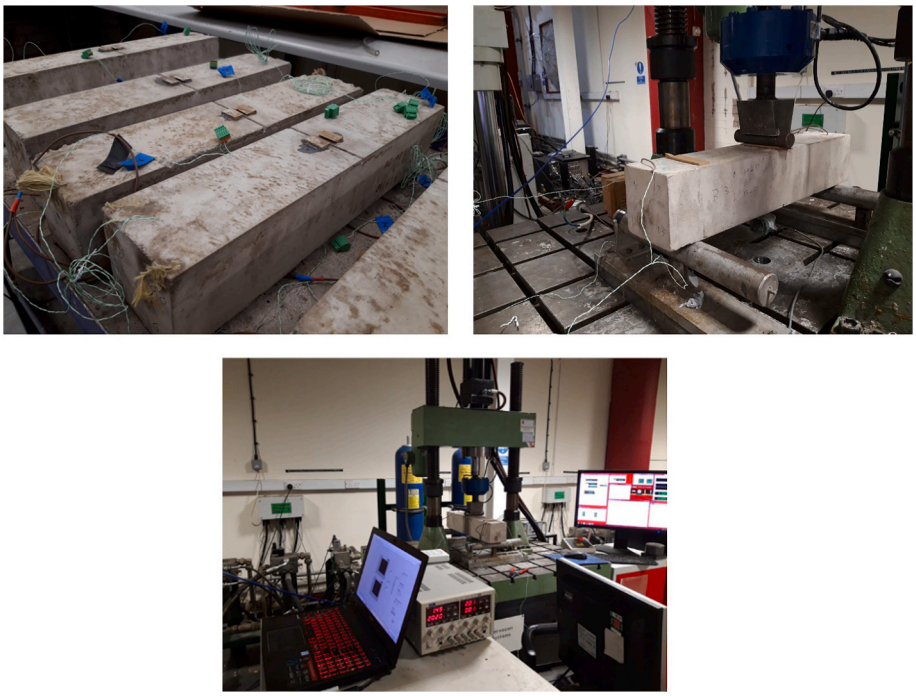

Fig. 8. Position of the CMOD sensors to measure the crack opening during the three-point bending test and experimental set-up.

turn provokes a reduction of the Load to the final value P_{red}.

A 5 mm notch was cut from the underside of all specimens, either side of which were stainless steel knife edges to accommodate the CMOD clip gauge (Fig. 8). A range of values spanning from 0.2 mm to 0.3 mm were targeted in order to explore the efficacy of the method under diverse grades of damage.

Stage 2: Once the desired CMOD is achieved ($CMOD_{BA}$), the loading machine was then switched from displacement control to Load control and the activation system was switched on while the Load stayed at the constant value of P_{red}. The activation process released the stress stored within the tendons, thereby generating a hogging bending Moment and closing the crack. In this stage the CMOD would show a reduction in the crack width from $CMOD_{BA}$ to $CMOD_{AA}$ due to the action of the hybrid tendons.

Stage 3: Once the crack has been closed and the specimen repaired under constant load, the machine was then switched to displacement control again and the load further increased. During this stage, an initial recovery of stiffness could be observed. The stiffness would gradually reduce as the crack opened again. The value of the Load associated to the crack reopening is reported in Fig. 8 as P_{reo} and it is also a measure of the effect of the post-compression from the tendons, which would in turn boost the overall flexural response of the structural element.

5. Numerical model

The non-linear beam-hinge model, presented in Balzano et al. (2021), has been enhanced to simulate the current experiments. Specifically, the model has been modified to allow the simulation of Stage 2 of the testing procedure (see Fig. 7). This accounted for the release of the tendon pre-stress and model the CMOD reduction at a constant external load level.

The theory assumes that the inelastic deformations are confined to a narrow central zone named the 'hinge' which can be associated with the fracture process zone (Karihaloo, 1996). The cementitious material is assumed to be linear prior to cracking and subsequently follows a damage-based evolution function, as explained below.

The central hinge is modelled as a layered beam (Owen and Hinton, 1980) under constant curvature and subject to a uniform bending moment and a normal force (crack-closure action from the Hybrid Tendons). The beam elements on either side of the hinge zone are assumed to be linear elastic beam elements.

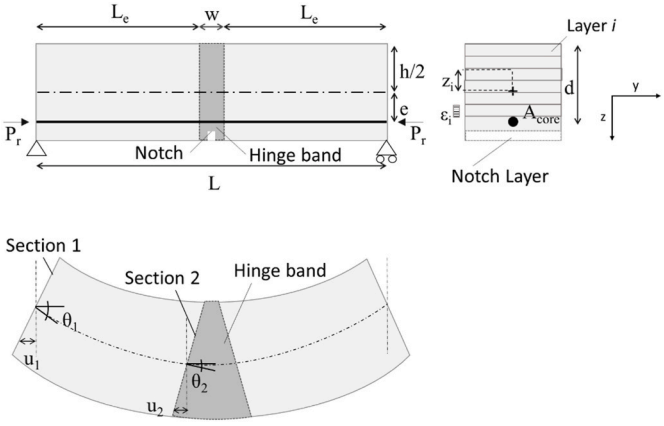

Fig. 9. Scheme of the Hinge Model and Layered beam.

The nonlinear stress-strain behavior of each layer is represented using a one-dimensional version of the basic damage model (Alnaas and Jefferson, 2016), which may be expressed as equation (1).

$$\sigma = (1 - \omega(\zeta))E\varepsilon \tag{1}$$

in which σ and ε are the uniaxial stress and strain in a layer respectively, E is Young's modulus of the mortar, $\omega \in [0,1]$ is the scalar damage variable, which is a function of the effective strain (ζ_i), as follows;

$$\omega(\zeta) = \begin{cases} 0 & if < \varepsilon_t \\ 1 - \dfrac{\varepsilon_t}{\zeta}\left[e^{-c_1\left(\frac{\zeta-\varepsilon_t}{\varepsilon_0-\varepsilon_t}\right)}\right] & if \zeta \geq \varepsilon_t \end{cases} \tag{2}$$

where c_1 is a softening parameter; ε_0 is the strain at the end of the

Table 2
Input paramenters for the numerical model.

b	H	w	e	n_{lay}	Δz	E_{core}	E_c	f_c	ε_{p0}	A_{core}	P_{r0}
mm	*mm*	*mm*	*mm*		*mm*	*MPa*	*MPa*	*MPa*		mm^2	*kN*
100	100	5	25	100	1	70,000[a]	30,000	30	0.0007	124.7	6.1

Note that P_{r0} is the initial pre-stress force stored within the inner core of the Hybrid tendons and is given by.
[a] The Elastic Modulus was taken from (Linear Composites Limited) for PARAFIL Type F which is the one used in this study.

softening curve and it is expressed as $\varepsilon_0 = u_0/w$; u_0 is the displacement at the end of the softening curve; and $\varepsilon_t = f_t/E_c$ is the tensile strain and f_t is the tensile strength of the concrete.

The effective strain (ζ_i) for a layer i is defined as the maximum axial strain (ε_i) experienced in the layer up to the time being considered; ε_i is expressed as follows:

$$\varepsilon_i = \overline{\varepsilon} + \Psi_c z_i = \overline{\varepsilon} - \frac{2\theta_2}{w} z_i \tag{3}$$

where $\overline{\varepsilon}$ is the axial strain at z = 0 in the hinge; Ψ_c is the hinge curvature, θ_2 is the rotation at one edge of the hinge zone; w is the width of the hinge band and z_i is the vertical coordinate for layer i, as illustrated in Fig. 9.

$$\theta_2 = -\frac{u_2}{L_e} \tag{4}$$

Where u_2 is the displacement at the hinge section and L_e is the length of the elastic beam element (Fig. 9).

The numerical model solves the equilibrium at the hinge cross-section between the internal normal Force N and momentum M and the external action applied by the tendons pre-stress once activated P_r. Each of the forces was calculated as the sum of the contributions from each layer of the hinge as per following

$$N = \int_{-\frac{h}{2}}^{\frac{h}{2}} \sigma_c b \, dz = \left(\sum_i E_{ci} b_i \Delta z_i \right) \varepsilon_i = -P_r \tag{5a}$$

$$M = \int_{-\frac{h}{2}}^{\frac{h}{2}} \sigma_c b z \, dz = \frac{PL}{4} - P_r e \tag{5b}$$

The tendon load is given by

$$P_r = A_p E_p \left(\varepsilon_{p0} - \frac{2u_{1p}}{L} \right) \tag{6}$$

with ε_{p0} being the initial pre-strain in the tendons' inner core.

Introducing the elastic beam segments between the supports and the hinges, applying compatibility at the interface between these two components, employing equations (1) and (3), and applying symmetry leads to the following coupled nonlinear equations, in which the primary unknowns are $\overline{\varepsilon}$ and θ_2.

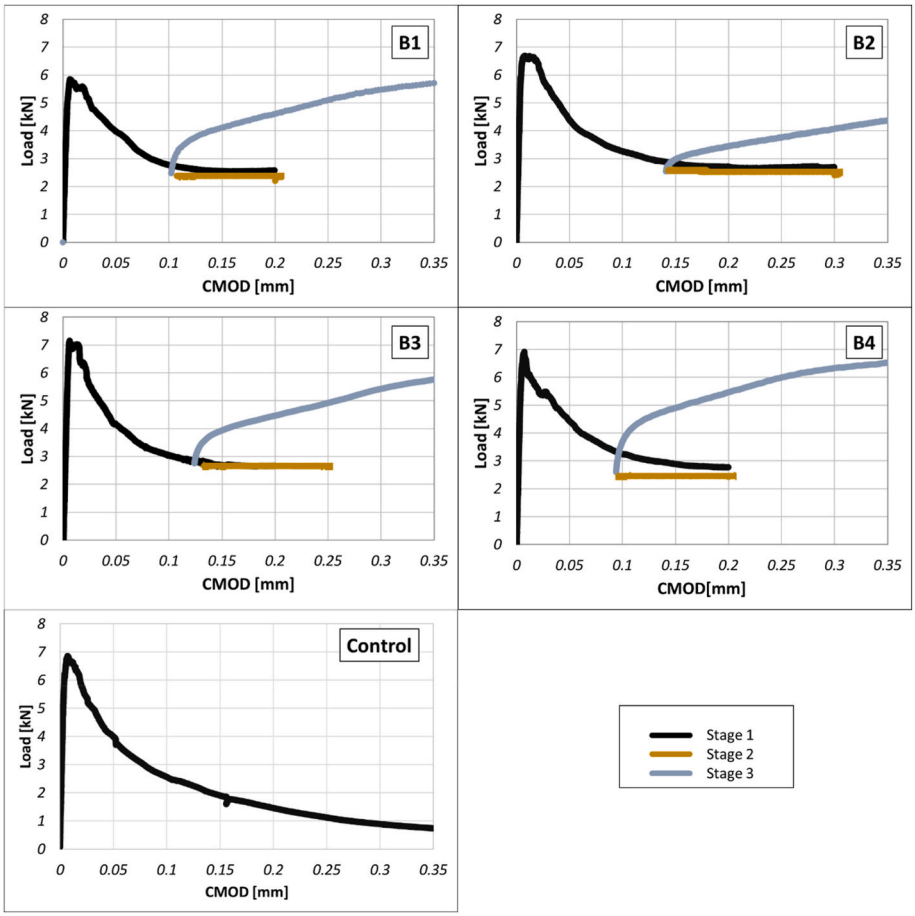

Fig. 10. Load-CMOD results for the three-point bending test carried out on the four concrete beams and the control beam (plain concrete).

Table 3
Output values from the experiments.

Specimen	P_{Peak}	P_{red}	$P_{reo\_measured}$	P_{r_reo}	P_{ult}	$CMOD_{ult}$	$P_{core,ult}$	$\sigma_{core,ult}$
	kN	*KN*	*kN*	*kN*	*kN*	*mm*	*kN*	*MPa*
B1	5.8	2.6	3.6	3.1	11.7	3.1	20.3	162.8
B2	6.7	2.7	2.9	0.6	10.1	1.9	17.4	139.4
B3	7.2	2.6	3.8	3.6	11.8	3.1	20.6	164.9
B4	6.9	2.5	4.3	5.4	12.2	2.6	21.2	169.8

$$\begin{bmatrix} N \\ M \end{bmatrix} = \begin{bmatrix} \sum_i E_{ci} b_i \Delta z_i + E_p A_p + \lambda_\varepsilon & \left(\sum_i E_{ci} b_i z_i \Delta z_i + z_i E_p A_p\right)\frac{2}{w} - \lambda_\theta \\ \sum_i E_{ci} b_i z_i \Delta z_i + E_p A_p z_p + \lambda_\varepsilon e & \frac{2}{w_c}\left(\sum_i E_{ci} b_i {z_i}^2 \Delta z_i + E_p A_p {z_p}^2\right) - \lambda_\theta e \end{bmatrix} \bullet \begin{bmatrix} \bar{\varepsilon} \\ \theta_2 \end{bmatrix} \tag{7}$$

where A_p is the area of the pre-stressed element, i.e. the cross section of the Kevlar® inner rope; E_p is Young modulus of the Kevlar® inner core; A_e is the area of the mortar beam outside the hinge band; E_e is Young modulus of the mortar outside the hinge band ; λ_{p0}, λ_ε, λ_θ, λ_P, κ_1, κ_2, κ_3 are the variables introduced by Balzano et al., 2021) and given by the following expressions:

$$\lambda_{p0} = A_p E_p \left(1 - \frac{2}{L}\kappa_3 \kappa_1\right) \tag{8}$$

$$\lambda_\varepsilon = A_p E_p \frac{2}{L}\kappa_3 \frac{w_c}{2} \tag{9}$$

$$\lambda_\theta = -\left(A_p E_p \frac{2}{L}\kappa_3 e\right) \tag{10}$$

$$\lambda_P = -\left(A_p E_p \frac{2}{L}\kappa_3 \kappa_2\right) \tag{11}$$

$$\kappa_1 = \frac{A_p E_p L_e}{E_e}\left(\frac{1}{A_e} + \frac{e^2}{I_e}\right) \tag{12}$$

$$\kappa_2 = -\frac{e}{E_e I_e}\frac{{L_e}^2}{4} \tag{13}$$

$$\kappa_3 = \frac{L}{L + 2\kappa_1} \tag{14}$$

The associated algorithm follows the same stages used in the testing procedure, as illustrated in Fig. 7. The nonlinear equations are solved using a standard Newton Raphson incremental iterative solution algorithm (de Souza Neto et al., 2011).

It is worth mentioning that in Stage 1, the tendons are not yet activated, hence ε_{p0} is assumed to be zero; however, once the tendons are activated, ε_{p0} is released (hence $\varepsilon_{p0} \neq 0$) and there is a step increase in the force P_r (given by equation (6)).

The model was coded in a Mathcad sheet (PTC Mathcad Prime 9.0), which was used for all the simulations reported into this paper. The general input parameters for the model are given in Table 2.

$$P_{r0} = \varepsilon_{p0} A_{core} E_{core} \tag{15}$$

where ε_{p0} is the initial strain of the Kevlar inner core due to the pre-stressing action, A_{core} is the Area of the inner core and E_{core} is the Kevlar Elastic Modulus (Linear Composites Limited) as reported in Table 2.

6. Results

6.1. Tendons activation

Fig. 10 and Table 3 show the results of the three-point bending test for the four specimens. The graph in Fig. 10 gives the Load-CMOD responses of each stage of the test. It is worth noticing that the experimental values for the three Stages of the tests are not continuous: this is

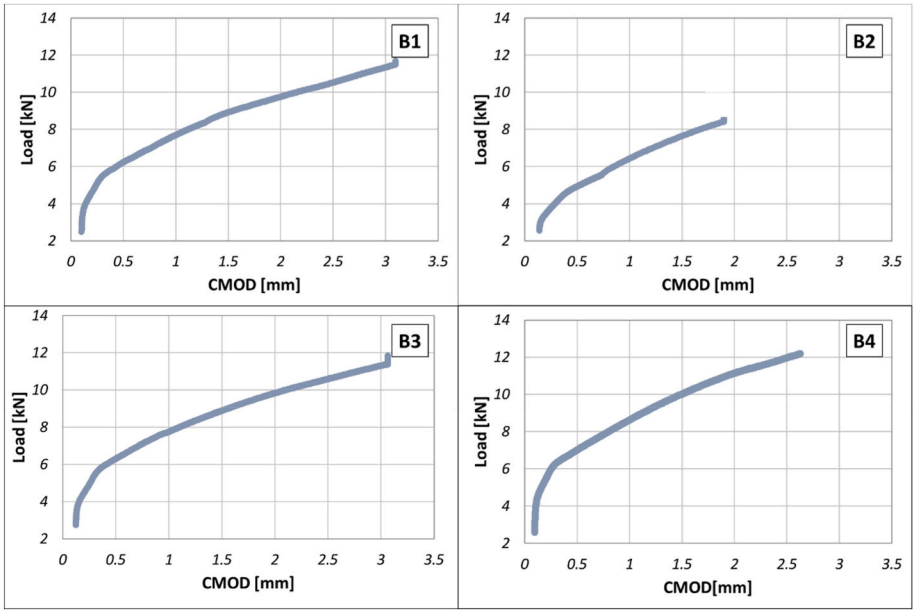

Fig. 11. Results at the ultimate state in Stage 3.

Table 4
Output values from the numerical model.

Specimen	c_1	u_0	$u_{2,\ stage1}$	$u_{2,\ stage3a}$	$u_{2,\ stage3b}$	$P_{reo\_modelled}$	$\sigma_{p0,loss}$	$\sigma_{p0,loss}/\sigma_{p0}$
			mm	*mm*	*mm*	*kN*	*MPa*	*%*
B1	0.85	0.035	0.268	0.136	0.4	3.4	12.9	26
B2	0.85	0.04	0.32	0.164	0.4	3.1	18.7	38
B3	0.87	0.035	0.32	0.164	0.4	3.7	11.6	24
B4	0.8	0.03	0.268	0.136	0.4	4.2	8.9	18

Table 5
Length of Tendons before and after the activation.

Length in mm	
Before Activation	*After Activation*
403	381
400	390
404	356

due to the fact that between the test stages the loading cell was stopped to switch from the displacement control to load control and to allow the switching of the power supply for the activation. During these pauses the values recorded by the machine showed a small fluctuation.

In Stage 1 of the experiment, the concrete beams showed an initial linear response, becoming nonlinear approaching the peak Load, after which all the specimen experienced a softening behavior provoking an average Load reduction of 49% compared to the Peak Load as also shown by the values for P_{red} reported in Table 3. The influence of the Kevlar reinforcement was not very evident during Stage 1 as shown by the softening behavior. It is possible that at this stage the tendons might be experiencing some slippage at the anchorages which was a problem already encountered in Balzano et al., 2021). However, the overall Load reduction was still lower compared to the one shown in Fig. 11 for plain concrete control beam, which confirms a reinforcement action from the Hybrid Tendons.

It is worth noting that B1 showed a lower value for P_{peak} compared to the other specimens although all made with the same mix design. This could be due to some human error made during the casting procedures (i.e. poor vibrating, little movement of tendons) which prevented the concrete flowing freely within the cross section, in turn influencing the flexural response of the element. The value recorded for P_{peak} is however still within 10% margin off the average value, which was considered an acceptable error.

The Load-CMOD response also shows that during Stage 2 the activation system successfully enabled the Hybrid Tendons to deliver the crack-closing action, by not only inducing a considerable reduction in crack width during Stage 2 (more details are discussed in Section 6.2) but also boosting the overall structural response after the activation. The measured values for P_{reo} also reflect the tendons efficiency after the activation. In particular, the fraction of original prestress force that remains after the crack-closure was estimated by computing the total prestress force associated with P_{reo} (P_{r_reo}):

$$P_{r\_reo} = \frac{1}{\left(\frac{1}{A_c} + \frac{e}{Z}\right)} \frac{M_{reo}}{Z} \tag{16}$$

where A_c is the Area of concrete, e is the eccentricity of the tendons system from the center of the beam, Z is the Section Modulus, and M_{reo} is the value of the bending moment associated to the recorded load P_{reo}.

The computed values for P_{r_reo} reported in Table 3 show that a considerable amount of the original Prestress remained and available at the onset of Stage 3.

The Load/CMOD values at the ultimate conditions reached at the end of Stage 3 are also reported in Fig. 11 and Table 5. In particular the stress

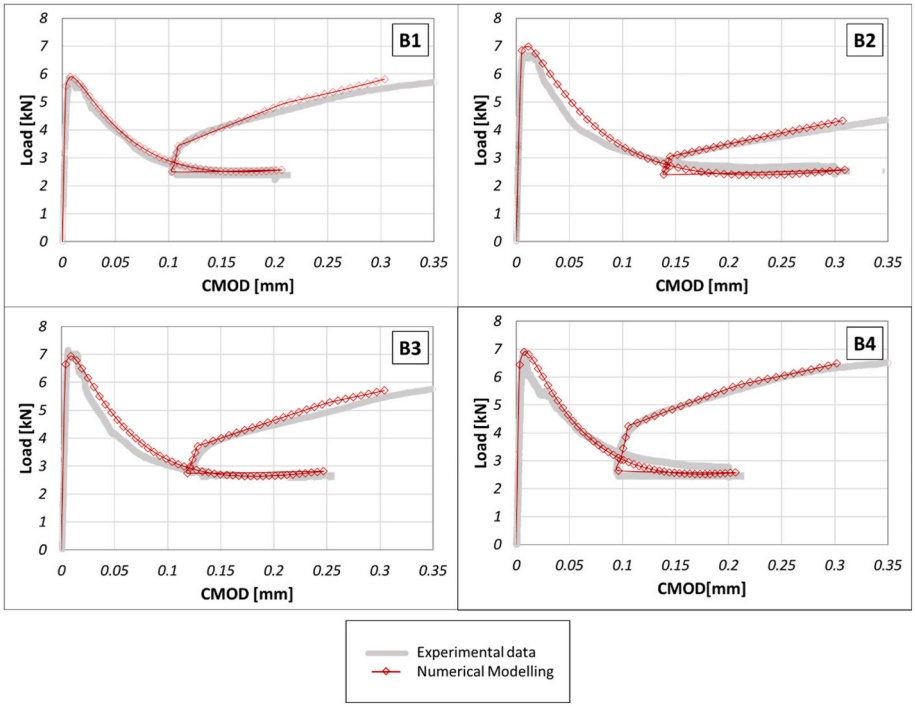

Fig. 12. Comparison between the results of the numerical model and the experimental values.

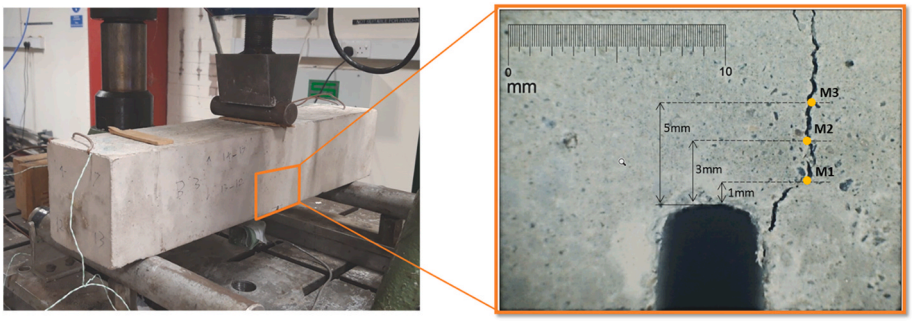

Fig. 13. Positions at which the crack width was measured via microscope before and after the activation of the Hybrid Tendons.

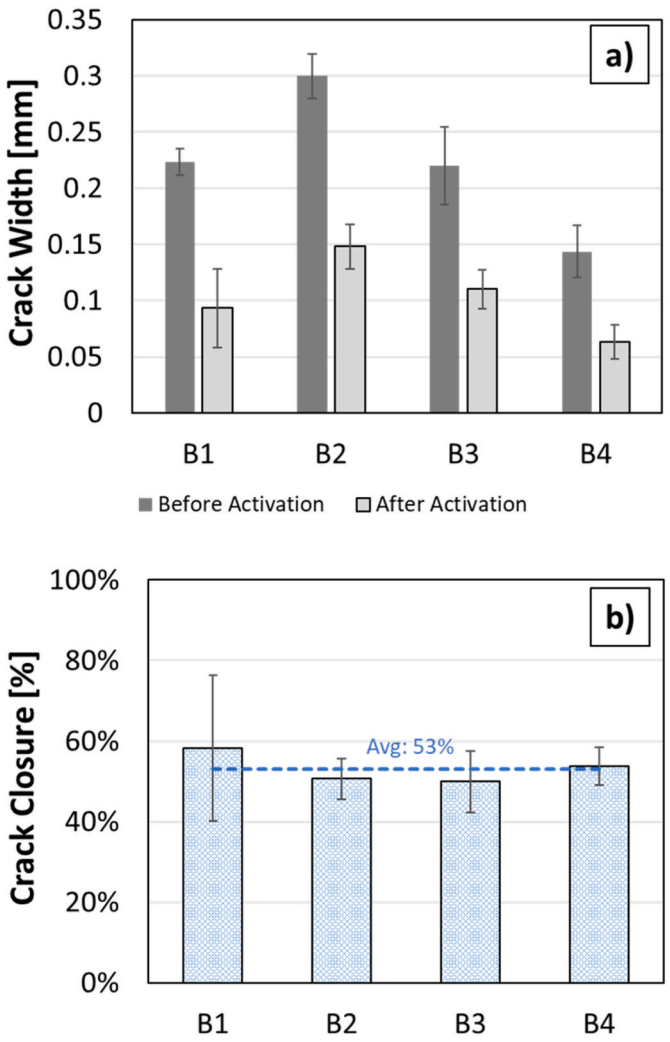

Fig. 14. a) Crack width measurements before and after the activation. b) Crack closure due to the post-compression action of the Hybrid Tendons.

within the Kevlar inner core at failure was estimated in order to check the working conditions compared with the nominal tensile strength (i.e. 600 MPa). It is evident that the Kevlar was working well below its limit state, therefore not used at its full potential.

Fig. 12 shows the comparison between the results of the numerical model and the experimental results. The numerical model was exploited to reproduce the crack-closure action and the effect of the compression after the activation on the overall structural response of the concrete specimens.

Table 4 reports the relevant output from the numerical model that were calibrated in order to match the experimental data. It can be noticed that the values of P_{reo} estimated from the numerical model ($P_{reo\_modelled}$) are quite consistent with the experimental values (see Table 3). Moreover, an estimation of the strain losses within the inner core of the Hybrid Tendons was made, showing that due to slippage at the anchorages position all the specimens experienced a reduction of the original pre-stress varying from 18 to 38% of the initial pre-stress. It is worth mentioning that the specimen B2 showed the highest losses as it was also the only one pushed to a higher value for $CMOD_{BA}$; this in turn also justifies the lowest value for P_{r_reo} for this specimen discussed previously in Table 3.

6.2. Crack-width measurements

The crack width on each specimen was also monitored using a Digital Microscope Camera (3in1 Type-C USB Portable) mounted close to the lateral face of each beam when sitting on the loading machine. The camera was mounted on pedestal and pointed perpendicularly on the surface of the concrete specimen to capture the crack. The pictures were used to then take measurements of the crack width at three different positions as reported in Fig. 13. Three measurements of the crack width were taken at 1 mm, 3 mm and 5 mm from the top of the notch. The average of the three measurements was taken.

The position chosen for the crack measurement is justified by the fact that the crack was developed under bending action: the crack front in turn develops in a way that the crack tip will always experience the greatest width. Therefore the values in proximity of the crack tip were used as reference point for the measurements to test the efficacy of the crack closure, assuming those values to be representative of the highest degree of damage experienced by the sample.

Fig. 14a shows the average crack width before and after the activation for each specimen. It is clearly visible how the tendons have contributed to a consistent crack width reduction. This result is even more encouraging if we consider that the action of the tendons was successful while the beam was still being loaded.

The hybrid tendons have contributed to achieving a crack reduction of up to 58% compared to its value before the activation. The average value for the crack closure among the samples is about 53% as reported also in Fig. 14b. These values are highly promising and would bring crack-width to values for which autogenous healing could take place (Yang et al., 2011), (Maes et al., 2016).

6.3. Temperature control

This section presents the values recorded by the thermocouples embedded in the concrete specimens and the correlation between temperature and crack closure size, highlighting that the tendons were successfully activated and the crack-closure action was successfully delivered.

Fig. 15 shows the recorded CMOD and the average recorded temperature from the three thermocouples for each specimen during

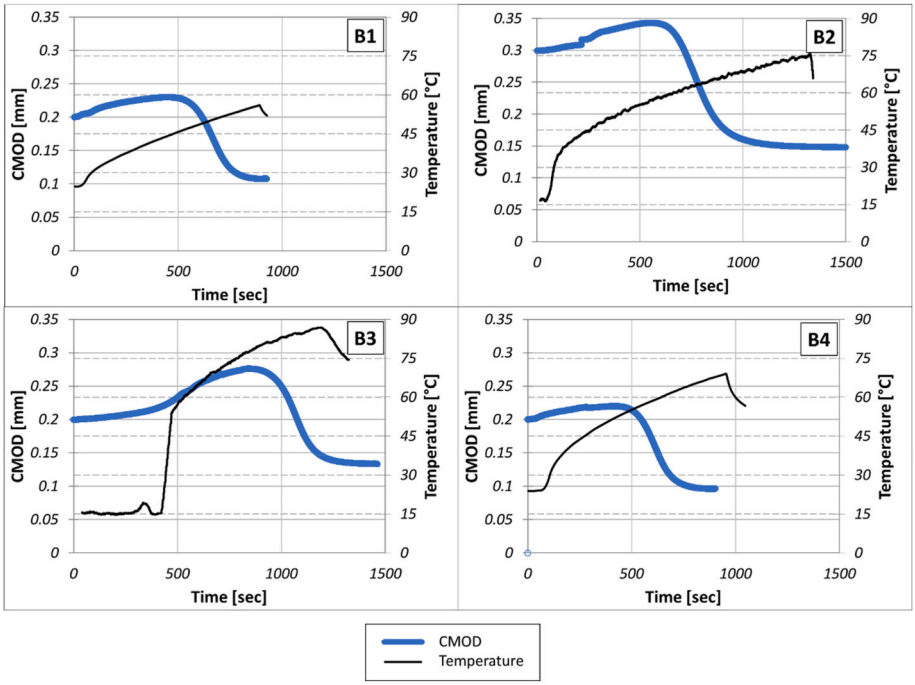

Fig. 15. Comparison between the monitored CMOD and the Temperature within the samples.

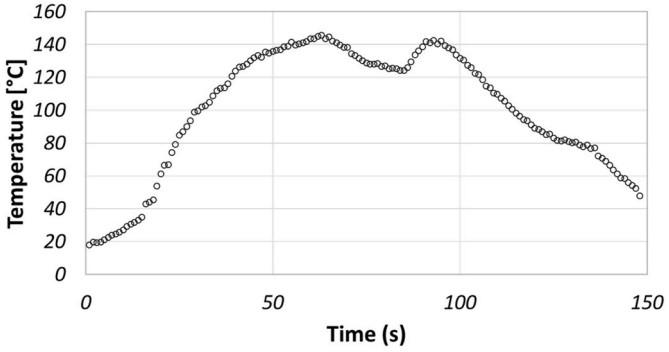

Fig. 16. Average Temperature during the activation process of the Tendons outside concrete.

activation. It is noticeable that the crack width gradually reduced with the increasing temperature. The values shown are strongly influenced by the vicinity of the thermocouple to the tendon itself. It is highly possible that during casting the sensors may have experienced a little movement, which in some cases could have been away from the tendon surface. Such a movement would have allowed some concrete paste to flow in between them. This would in turn lead to a slower response of the sensor.

The results showed that crack aperture started reducing when the temperature reached the range 45–75 °C, confirming that the activation process might start around these values.

In order to further explore the performance of the activation system an experiment of activation outside the beam was also performed. Three tendons with the same geometry and characteristics of the ones presented for the concrete specimens, were wrapped with Kanthal wires and connected to the power supply. A thermocouple was also attached to the tendons to monitor the temperature change during the activation process. Table 5 reports the values of the tendons' length before and after the activation.

Fig. 16 shows also the average monitored temperature of the PET sleeve during the activation process. The test showed that the system was appropriate to supply the right energy amd activate the polymer hence releasing the pre-stress stored within the Kevlar core.

7. Conclusions

The present study expands and improves upon the Hybrid Tendon system, which was originally introduced in concrete beams as a self-closing crack mechanism in the research conducted by Balzano et al. (Wu et al., 2012). This investigation introduces an electric heating system specifically designed for this purpose, seamlessly integrated into the concrete elements. The system autonomously triggers the tendons within the concrete, closing cracks by selectively applying heat exclusively to the tendons and the adjacent section of the element in contact with them. The system, employing Kanthal wires, ensures the accurate activation of the tendons, especially when the concrete elements that are integral to the structure are under load.

The effectiveness of crack closure was assessed through a three-point bend test, comparing the mechanical behaviour of concrete samples containing four tendons with control samples. Experimental results were used to calibrate a numerical model, demonstrating its capability to reproduce the results.

From the analyses of the results presented in the paper, the following main conclusions can be drawn.

- the inclusion of tendons with the integrated heating system does not appear to affect the flexural strength of the beams in stage 1 (undamaged state).
- the activation of the crack-closing system occurred when the structure is under load, simulating a real-case scenario.
- the proposed activation system successfully provided enough heating power to activate the outer PET sleeve, hence releasing the prestress potential stored within the tendons system to close serviceability level cracks (0.3 mm) in concrete beam specimens. Crack-width measurements, reveal a remarkable reduction, reaching up to 58% after activation.
- preservation of original prestress within the tendons ranged between 50% and 90% after activation when the crack closure target was

below 0.15 mm. This preservation significantly enhanced the overall flexural strength of the concrete beam.
- Hybrid Tendons acted as effective reinforcement, demonstrating the ability to withstand the ultimate state of loading. The reinforcing effect became more pronounced after activation, potentially due to slippage at the anchorages, as confirmed by numerical modelling.
- the model was able to reproduce the crack-closure action and the overall efficiency of the Hybrid Tendon after the activation process.
- the model allowed estimation of potential slippage at the anchorages, resulting in a loss of the original pre-stress stored within the inner core ranging between 18 and 38%.

In summary, the integration of Hybrid Tendons with a dedicated electric heating system demonstrates significant potential for enhancing the durability and service life of concrete structures. The findings encourage further research and development in the pursuit of innovative solutions for mitigating concrete cracking and promoting sustainable infrastructure practices. Future studies will focus on examining the behaviour at the anchorages for a comprehensive understanding of the system's performance.

CRediT authorship contribution statement

Brunella Balzano: Writing – review & editing, Writing – original draft, Visualization, Supervision, Software, Project administration, Methodology, Investigation, Funding acquisition, Data curation, Conceptualization. **Shahram Sharifi:** Writing – review & editing, Writing – original draft, Validation, Software, Investigation, Formal analysis, Data curation, Conceptualization. **John Sweeney:** Writing – review & editing, Resources. **Glen Thompson:** Resources, Investigation. **Cristina de Nardi:** Writing – review & editing, Supervision, Methodology, Investigation, Funding acquisition. **Tony Jefferson:** Writing – original draft, Validation, Supervision, Software, Project administration, Funding acquisition, Conceptualization.

Declaration of competing interest

The authors declare that they have no known competing financial interests or personal relationships that could have appeared to influence the work reported in this paper.

Data availability

Data will be made available on request.

Acknowledgement

This work is supported by UKRI-EPSRC (Grant No. EP/P02081X/1, Resilient Materials 4 Life, RM4L). This research was funded also by the Leverhulme Trust ECF-2022-235.

Data associated with research published and support information in this paper are at http://doi.org/10.17035/d.2024.0319308757.

References

Alexander, M.G., 2018. Service life design and modelling of concrete structures – background, developments, and implementation. Revista ALCONPAT 8 (3), 224–245. https://doi.org/10.21041/ra.v8i3.325.

Alexander, M., Beushausen, H., 2019. Durability, service life prediction, and modelling for reinforced concrete structures – review and critique. Cement Concr. Res. 122, 17–29. https://doi.org/10.1016/j.cemconres.2019.04.018. Elsevier Ltd.

Alnaas, W.F., Jefferson, A.D., 2016. A smooth unloading-reloading approach for the nonlinear finite element analysis of quasi-brittle materials. Eng. Fract. Mech. 152, 105–125. https://doi.org/10.1016/j.engfracmech.2015.04.018.

Althoey, F., et al., 2022. Machine learning based computational approach for crack width detection of self-healing concrete. Case Stud. Constr. Mater. 17 (Dec) https://doi.org/10.1016/j.cscm.2022.e01610.

Angst, U., 2019. Durable concrete structures: cracks & corrosion and corrosion & cracks. International Association for Fracture Mechanics of Concrete and Concrete Structures. https://doi.org/10.21012/fc10.233307.

Balzano, B., Sweeney, J., Thompson, G., Tuinea-Bobe, C.L., Jefferson, A., 2021. Enhanced concrete crack closure with hybrid shape memory polymer tendons. Eng. Struct. 226, 111330 https://doi.org/10.1016/J.ENGSTRUCT.2020.111330.

Bekas, D.G., Tsirka, K., Baltzis, D., Paipetis, A.S., 2016. Self-healing materials: a review of advances in materials, evaluation, characterization and monitoring techniques. Compos. B Eng. 87, 92–119. https://doi.org/10.1016/J.COMPOSITESB.2015.09.057.

Beushausen, H., Torrent, R., Alexander, M.G., 2019. Performance-based approaches for concrete durability: state of the art and future research needs. Cement Concr. Res. 119, 11–20. https://doi.org/10.1016/j.cemconres.2019.01.003.

Cappellesso, V.G., Van Mullem, T., Gruyaert, E., Van Tittelboom, K., De Belie, N., 2023. Bacteria-based self-healing concrete exposed to frost salt scaling. Cem. Concr. Compos., 105016 https://doi.org/10.1016/j.cemconcomp.2023.105016.

Chang, C., Ho, M., Song, G., Mo, Y.L., Li, H., 2009. A feasibility study of self-heating concrete utilizing carbon nanofiber heating elements. Smart Mater. Struct. 18 (12) https://doi.org/10.1088/0964-1726/18/12/127001.

CHT UK Bridgwater LTD, "Technical Data Sheet- AS1803- SILCOTHERM 1 Part RTV Silicone Adhesive Sealant Paste Non Corrosive.".

Dai, L., Bian, H., Wang, L., Potier-Ferry, M., Zhang, J., 2020. Prestress loss Diagnostics in Pretensioned concrete structures with corrosive cracking. J. Struct. Eng. 146 (3) https://doi.org/10.1061/(asce)st.1943-541x.0002554.

Danish, A., Mosaberpanah, M.A., Salim, M.U., 2020. Past and present techniques of self-healing in cementitious materials: a critical review on efficiency of implemented treatments. J. Mater. Res. Technol. 9 (3), 6883–6899. https://doi.org/10.1016/J.JMRT.2020.04.053.

Dawood, T., Zhu, Z., Zayed, T., 2020. Deterioration mapping in subway infrastructure using sensory data of GPR. Tunn. Undergr. Space Technol. 103 https://doi.org/10.1016/j.tust.2020.103487.

De Belie, N., et al., 2018. A review of self-healing concrete for damage Management of structures. Adv. Mater. Interfac. 5 (17) https://doi.org/10.1002/admi.201800074. Wiley-VCH Verlag.

de Rooji, M., van Tittelboom, T., De Belie, N., Schlangen, E., 2013. Self-Healing Phenomena in Cement-Based Materials, vol. 11. Springer.

De Nardi, C., Gardner, D., Cristofori, D., Ronchin, L., Vavasori, A., Jefferson, T., 2023. Advanced 3D printed mini-vascular network for self-healing concrete. Mater. Des. 230 https://doi.org/10.1016/j.matdes.2023.111939.

de Souza Neto, E.A., Peric, D., Owen, D.R.J., 2011. Computational Methods For Plasticity: Theory and Applications. John Wiley & Sons.

Dolan, W., 1991. Kevlar reinforced prestressing Bridge Decks. Transport. Res. Rec. 1, 68–76.

Edvardsen, C., 1999. Water permeability and autogenous healing of cracks in concrete. ACI Materials Journal – American Concrete Institute 96 (4), 448–454.

Edvardsen, C., Dhir, R.K., Jones, M.R., 2015. Water PERMEABILITY and autogenous HEALING OF cracks IN concrete. https://doi.org/10.1680/iicsdac.28241.0047.

Gupta, S., Kua, H.W., Pang, S.D., 2018. Healing cement mortar by immobilization of bacteria in biochar: an integrated approach of self-healing and carbon sequestration. Cem. Concr. Compos. 86, 238–254. https://doi.org/10.1016/J.CEMCONCOMP.2017.11.015.

Han, B., et al., 2015. Smart concretes and structures: a review. J. Intell. Mater. Syst. Struct. 26 (11), 1303–1345. https://doi.org/10.1177/1045389X15586452. SAGE Publications Ltd.

Hossain, M.R., Sultana, R., Patwary, M.M., Khunga, N., Sharma, P., Shaker, S.J., 2022. Self-healing concrete for sustainable buildings. A review. Environ. Chem. Lett. 20 (2), 1265–1273. https://doi.org/10.1007/s10311-021-01375-9. Springer Science and Business Media Deutschland GmbH.

Jefferson, A., Joseph, C., Lark, R., Isaacs, B., Dunn, S., Weager, B., 2010. A new system for crack closure of cementitious materials using shrinkable polymers. Cement Concr. Res. 40 (5), 795–801. https://doi.org/10.1016/j.cemconres.2010.01.004.

Kanthal, A.B., 2003. *KANTHAL HANDBOOK - Heating Alloys for Electric Household Appliances*. Primatryck [Online]. Available: www.kanthal.com.

Karihaloo, B.L., 1996. Fracture mechanics and structural concrete. Int. J. Fract. 77.

Kumar Jogi, P., Vara Lakshmi, T.V.S., 2021. Self healing concrete based on different bacteria: a review. Mater. Today Proc. 43, 1246–1252. https://doi.org/10.1016/J.MATPR.2020.08.765.

Kwan, A.K., Chen, J., Ng, P., Fung, W., 2013. Adding limestone fines, fly ash and silica fume to reduce heat generation of concrete. Mag. Concr. Res. 65, 865–877.

Linear Composites Limited, "Parafil-The Ultimate Synthetic Rope Technical Note," Keighley..

Maes, M., Snoeck, D., De Belie, N., 2016. Chloride penetration in cracked mortar and the influence of autogenous crack healing. Construct. Build. Mater. 115, 114–124.

Medeiros-Junior, R.A., 2018. Impact of climate change on the service life of concrete structures. In: Eco-efficient Repair and Rehabilitation of Concrete Infrastructures. Elsevier Inc., pp. 43–68. https://doi.org/10.1016/B978-0-08-102181-1.00003-4

Mindess, S., Young, F.J., Darwin, D., 2003. Concrete. In: Prentice Hall, second ed. Pearson Education, Inc., Upper Saddle River, NJ 07458, U.S.A.

Minnebo, P., et al., 2017. A novel design of autonomously healed concrete: towards a vascular healing network. Materials 10 (1). https://doi.org/10.3390/ma10010049.

Neville, A., 2002. " autogenous healing—a concrete Miracle?,". Concr. Int. 24 (11), 76–82.

Owen, D.R.J., Hinton, E., 1980. Finite elements in plasticity: theory and practice. Swansea. Pineridge Press Ltd.

Sales, A., De Souza, F.R., Dos Santos, W.N., Zimer, A.M., Almeida, F.D.C.R., 2010. Lightweight composite concrete produced with water treatment sludge and sawdust:

thermal properties and potential application. Construct. Build. Mater. 24 (12), 2446–2453. https://doi.org/10.1016/j.conbuildmat.2010.06.012.
Shen, Y., Yang, H., Xi, J., Yang, Y., Wang, Y., Wei, X., 2020. A novel shearing fracture morphology method to assess the influence of freeze–thaw actions on concrete–granite interface. Cold Reg. Sci. Technol. 169, 102900 https://doi.org/10.1016/J.COLDREGIONS.2019.102900.
Shields, Y., et al., 2024. Non-destructive evaluation of ductile-porous versus brittle 3D printed vascular networks in self-healing concrete. Cem. Concr. Compos. 145 (Jan) https://doi.org/10.1016/j.cemconcomp.2023.105333.
Teall, O., et al., 2018a. A shape memory polymer concrete crack closure system activated by electrical current. Smart Mater. Struct. 27 (7) https://doi.org/10.1088/1361-665X/aac28a.
Teall, O., et al., 2018b. A shape memory polymer concrete crack closure system activated by electrical current. Smart Mater. Struct. 27 (7) https://doi.org/10.1088/1361-665X/aac28a.
Vaysburd, A.M., Emmons, P.H., Mailvaganam, N.P., McDonald, J.E., Bissonnette, B., 2004. Concrete repair technology—a Revised approach is needed. Concr. Int. 26 (1), 58–65.
Wiktor, V., Jonkers, H.M., 2011. Quantification of crack-healing in novel bacteria-based self-healing concrete. Cem. Concr. Compos. 33 (7), 763–770. https://doi.org/10.1016/j.cemconcomp.2011.03.012.
Wu, M., Johannesson, B., Geiker, M., 2012. A review: self-healing in cementitious materials and engineered cementitious composite as a self-healing material. Construct. Build. Mater. 28 (1), 571–583. https://doi.org/10.1016/j.conbuildmat.2011.08.086.
Yang, Y., Yang, E.-H., Li, V.C., 2011. Autogenous healing of engineered cementitious composites at early age. Cement Concr. Res. 41 (2), 176–183.
Yildirim, G., Şahmaran, M., Anil, Ö., 2018. Engineered cementitious composites-based concrete. Eco-efficient Repair and Rehabilitation of Concrete Infrastructures 387–427. https://doi.org/10.1016/B978-0-08-102181-1.00015-0.